Front. Phys., 2014, 9(1): 3–16
DOI 10.1007/s11467-013-0356-2

PERSPECTIVE

Plasmon point spread functions: How do we model plasmon-mediated emission processes?

Katherine A. Willets

Department of Chemistry, University of Texas at Austin,
Welch Hall 1.202, 105 E 24TH ST. STOP A5300, Austin, TX 78712, USA
E-mail: kwillets@cm.utexas.edu

Received April 1, 2013; accepted May 30, 2013

A major challenge with studying plasmon-mediated emission events is the small size of plasmonic nanoparticles relative to the wavelength of light. Objects smaller than roughly half the wavelength of light will appear as diffraction-limited spots in far-field optical images, presenting a significant experimental challenge for studying plasmonic processes on the nanoscale. Super-resolution imaging has recently been applied to plasmonic nanosystems and allows plasmon-mediated emission to be resolved on the order of ~5 nm. In super-resolution imaging, a diffraction-limited spot is fit to some model function in order to calculate the position of the emission centroid, which represents the location of the emitter. However, the accuracy of the centroid position strongly depends on how well the fitting function describes the data. This Perspective discusses the commonly used two-dimensional Gaussian fitting function applied to super-resolution imaging of plasmon-mediated emission, then introduces an alternative model based on dipole point spread functions. The two fitting models are compared and contrasted for super-resolution imaging of nanoparticle scattering/luminescence, surface-enhanced Raman scattering, and surface-enhanced fluorescence.

Keywords plasmon, point spread function, dipole, super-resolution, surface-enhanced Raman scattering (SERS)

PACS numbers 81, 82

Contents

1 Introduction

Noble metal nanoparticles have long attracted researchers due to their unique interactions with light, through the excitation of localized or propagating surface plasmons [1–3]. Plasmons are the light-driven collective oscillation of surface conduction electrons in materials with a small positive imaginary and negative real dielectric function. Interest in plasmons derives from the diverse array of applications available, including waveguiding, optical trapping, sensing, and surface-enhanced spectroscopies such as surface-enhanced Raman scattering (SERS) and surface-enhanced fluorescence [3–13]. In surface-enhanced spectroscopy, molecules located on or near the surface of the plasmonic nanostructure are excited by plasmonically-enhanced electromagnetic fields at the nanoparticle surface; these fields may be locally enhanced by 10–10^4 depending on the nanoparticle structure, generating a corresponding enhancement of the

Frontiers of Physics

spectroscopic signal from the nearby molecule [10, 11].

Because the plasmonic properties of a nanoparticle depend strongly on its size and shape, many researchers have performed experiments relating the optical properties of the nanoparticle to its nanoscale structure [14–17]. However, one major challenge with these experiments is the small size of the nanoparticle relative to the diffraction-limit of light. Any object smaller than roughly half the wavelength of light will appear as a diffraction-limited spot when imaged with a far-field optical microscope. Figure 1 shows an example of a gold nanorod, imaged with both scanning electron microscopy [SEM, Fig. 1(a)] as well as dark-field imaging [Fig. 1(b)]. Unlike the SEM image, the shape of the nanorod cannot be determined from the optical image, and all information relating the optical scattering from the nanorod to its underlying structure is completely obscured. This problem is even more dramatic in plasmon-mediated molecular emission processes, such as SERS or surface-enhanced fluorescence. In these cases, both the molecule and the nanoparticle are smaller than the diffraction limit, so it is not possible to resolve the shape of the nanoparticle or the position/orientation of the molecule on its surface.

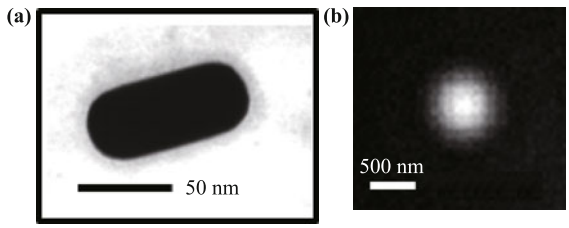

Fig. 1 **(a)** SEM image of a gold nanorod. **(b)** Dark-field scattering image of a gold nanorod, illustrating the challenge of the diffraction limit of light.

Recently, a far-field optical imaging technique known as super-resolution imaging has been used to overcome the diffraction limit of light and optically image plasmonic nanoparticles with nanoscale resolution [18–34]. In super-resolution imaging, a diffraction-limited image is fit to some model function, typically a two-dimensional (2D) Gaussian, in order to extract some parameter(s) of interest [35, 36]. Most often, the centroid position of the emission is extracted from the fit, as this represents the location of the emitter. Using this approach, the position of the emitter can be determined with resolution better than 5 nm, which is over an order of magnitude better than the diffraction-limited resolution [36, 37]. It is worth noting that super-resolution imaging is one of several sub-diffraction limited optical imaging techniques available, in addition to near-field scanning optical microscopy (NSOM), stimulated emission depletion (STED), and structured illumination microscopy (SIM) [38–41]. However, super-resolution imaging does not require a (potentially perturbative) scanning probe (as in NSOM) nor external manipulation of the excitation source (as in STED or SIM), which makes it a simple and relatively straightforward method for overcoming the diffraction-limit of light.

One challenge in super-resolution imaging is the choice of the fitting function used to model the diffraction-limited spot. In all reports of super-resolution imaging of plasmonic nanoparticles to date, a 2D Gaussian is used as the fitting function. However, the actual shape of the diffraction-limited spot is a complex convolution between the angular distribution of emission from the emitter at or near an interface, and the light collection properties of the imaging optics [42–46]. The actual shape of the emission spot, known as the point spread function (PSF), may not be well-represented by a 2D Gaussian, which can introduce error in the determination of the centroid position [45, 46]. This potential lack of centroid localization accuracy represents a significant challenge in the super-resolution imaging field at large.

This Perspective will compare and contrast the 2D Gaussian fitting approach with an alternative approach based on modeling the PSF of a dipole emitter. In Section 2, we will introduce super-resolution imaging and show several examples in which the 2D Gaussian model has been successfully applied to the study of plasmonic nanostructures. In Section 3.1, we introduce the dipole PSF model and discuss why it is superior for localizing emission from a single dipole. Next, we will compare the two models for three different plasmon-mediated emission scenarios: (i) direct nanoparticle emission via scattering or luminescence, (ii) plasmon-mediated molecular emission via SERS, and (iii) plasmon-mediated molecular emission via surface-enhanced fluorescence. In all cases, we will consider whether the dipole PSF model is appropriate for the system under study and describe the associated complexities of applying the PSF model over the 2D Gaussian. Because this field is only several years old (the first report of super-resolution imaging of a plasmonic nanostructure was published in 2010) [18], this Perspective is intended to stimulate further discussion and discovery of how best to apply super-resolution imaging methods to highly complex, coupled molecule-plasmon systems.

2 Super-resolution imaging of plasmon-mediated emission

2.1 Principle of super-resolution imaging

As discussed in the introduction, the preferred model for

fitting the emission of a sub-wavelength object is a 2D Gaussian, as shown in Eq. (1):

$$I(x,y) = z_0 + I_0 e^{-\frac{1}{2}\left[\left(\frac{x-x_0}{s_x}\right)^2+\left(\frac{y-y_0}{s_y}\right)^2\right]} \quad (1)$$

In this expression, $I(x,y)$ represents the intensity of the diffraction-limited spot as a function of position, z_0 is the intensity of the background, I_0 is the peak intensity of the diffraction-limited spot, s_x and s_y are the widths of the Gaussian, and x_0 and y_0 represent the centroid position. The centroid position is the primary parameter of interest because it represents the location of the emitter. With sufficient signal-to-noise, the location of the emitter can be determined with precision better than 5 nm using this approach [36, 37].

When multiple species are emitting simultaneously, the PSF will be a super-position of all emitters. To resolve each emitter uniquely, we need a way to modulate the emission, such that only one emitter is on at a time [35]. If we can do this, then we can fit the single active emitter and localize its centroid position. Repeating this process as individual emitters turn on and off over time allows the position of each emissive species to be localized [47, 48]. A super-resolution image is then constructed from the results of each fit by plotting the centroid positions of each emitter. Signal modulation is accomplished via a host of different mechanisms, including the use of light-driven photoswitchable probes [47, 48], the exploitation of "blinking" inherent to many emitters (such as quantum dots, or single molecule SERS signals) [18, 49], or the shelving of molecules into dark triplet states (known as ground state depletion) [50, 51]. By modulating emission from different species and fitting the PSF of each one individually, super-resolution images can be constructed that offer resolution at least an order of magnitude better than a traditional diffraction-limited image.

2.2 Examples of super-resolution images from plasmon-mediated emission

Super-resolution imaging of plasmonic nanoparticles falls into two categories: direct imaging of signals from the nanoparticle itself (e.g. scattering or luminescence) [20, 23, 25, 27, 33] or plasmon-mediated emission from molecules at or near the surface of the nanoparticle [18, 19, 21, 26, 28–32, 34]. One example of the former approach is called *photo*stable *o*ptical *n*anoscopy, or PHOTON [20]. In PHOTON, multiple nanoparticles within a diffraction-limited spot can be resolved based on differences in their scattering spectra. First, a series of dark field scattering images are collected with each image corresponding to scattering at a different wavelength. Next, each image is fit to a 2D Gaussian to extract the wavelength-dependent centroid position. By repeating this process over multiple image frames, it is possible to reconstruct the position of each individual nanoparticle within a single diffraction-limited spot. As a proof-of-principle, four biotinylated silver nanoparticles were bound to the four binding sites of streptavidin, creating a nanoparticle tetramer with fixed spacing between each nanoparticle. The resulting PHOTON images show that each nanoparticle within the tetramer is uniquely resolved, with the reconstructed inter-particle distances of 8–9 nm in strong agreement with the predicted spacing based on the size of the streptavidin molecule [20].

For super-resolution imaging of plasmon-mediated emission from molecules at or near the nanoparticle surface, three different approaches have been employed: (i) measuring surface-enhanced fluorescence from molecules spaced from the nanoparticle surface using surface-bound ligands [26, 34], (ii) imaging surface-enhanced fluorescence from solute molecules that diffuse near the surface of the plasmonic nanostructure [19, 30-32], and (iii) tracking SERS from molecules physisorbed on the surface of the nanoparticle [18, 21, 28, 29, 52]. The results of the various plasmonic super-resolution studies have yielded diverse insight into the structures of plasmonic nanoparticles [26, 34]; shape, size, and electromagnetic field enhancements of plasmonic "hot spots;" [18, 19, 21, 29, 32] and local catalytic activity at the surface of plasmonic nanoparticles [30, 31].

Figure 2 shows an example in which the shape of a plasmonic nanostructure is determined by fitting the PSFs of fluorescent species spaced from the nanoparticle surface using a surface-bound ligand [34]. In this example, a gold nanowire is used as a substrate, which has an extended dimension along its length (~2 μm) and a sub-diffraction-limited width (~70 nm). The inability of traditional far-field imaging [as in Fig. 2(a)] to accurately reproduce the width of the nanowire [Fig. 2(c)] is obvious. However, by fitting the position of individual carboxytetramethyl rhodamine (TAMRA) fluorophores attached to the nanowire surface with double stranded DNA, we can reconstruct the shape of the underlying nanowire using super-resolution imaging [Fig. 2(b)] and find that the dimensions agree extremely well with the actual structure, as determined by SEM [Fig. 2(d)] [34].

Figure 3 shows several examples of using super-resolution imaging to reconstruct the shape and electromagnetic enhancement associated with a plasmonic hot spot (e.g. regions of sizable electromagnetic field enhancement between adjacent nanoparticles). In the example shown in Fig. 3(a), individual fluorescent

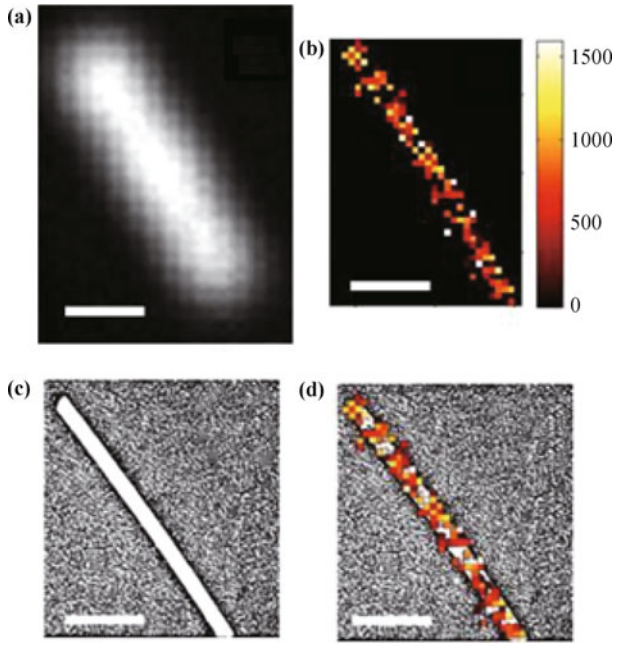

Fig. 2 **(a)** Dark-field image of a gold nanowire. **(b)** Reconstructed super-resolution image using fluorescence bursts from bound fluorophores. **(c)** SEM image of the nanowire, contrasted to emphasize the edges. **(d)** Overlay of super-resolution image on the SEM image showing dimensional agreement. All images have a common 500 nm scale bar. Adapted with permission from Ref. [34], Copyright © 2012 Royal Society of Chemistry.

molecules diffuse to the surface of a silver nanoparticle aggregate; when the molecule enters the hot spot, a burst of fluorescence is observed, which is fit to a 2D Gaussian [19]. By measuring the position of each fluorescent burst and correlating it with the intensity of the fluorescence, an image of the hot spot can be reconstructed. The hot spot has dimensions of 13.2 nm × 20.3 nm, and shows an exponential decay profile in intensity as the centroid position moves away from the region of peak intensity. Figure 3(b) shows a similar result, using SERS from a physisorbed analyte to map out the hot spot [21]. As with the previous result, the hot spot shows a region of peak intensity, accompanied by an exponential decay in intensity as the centroid position shifts away from the region of peak intensity. In this example, a correlated SEM image was also obtained [Fig. 3(c)], allowing us to match the shape of the hot spot with the structure of the SERS-active nanoparticle aggregate [Fig. 3(d)]. We note that the size and the shape of the hot spot map shows excellent agreement with the leftmost junction region of the nanoparticle aggregate, suggesting that this is the site being probed by the SERS reporter molecule.

While these examples are not meant to be exhaustive, they highlight the power of applying super-resolution imaging to plasmonic nanoparticles. Moreover, the

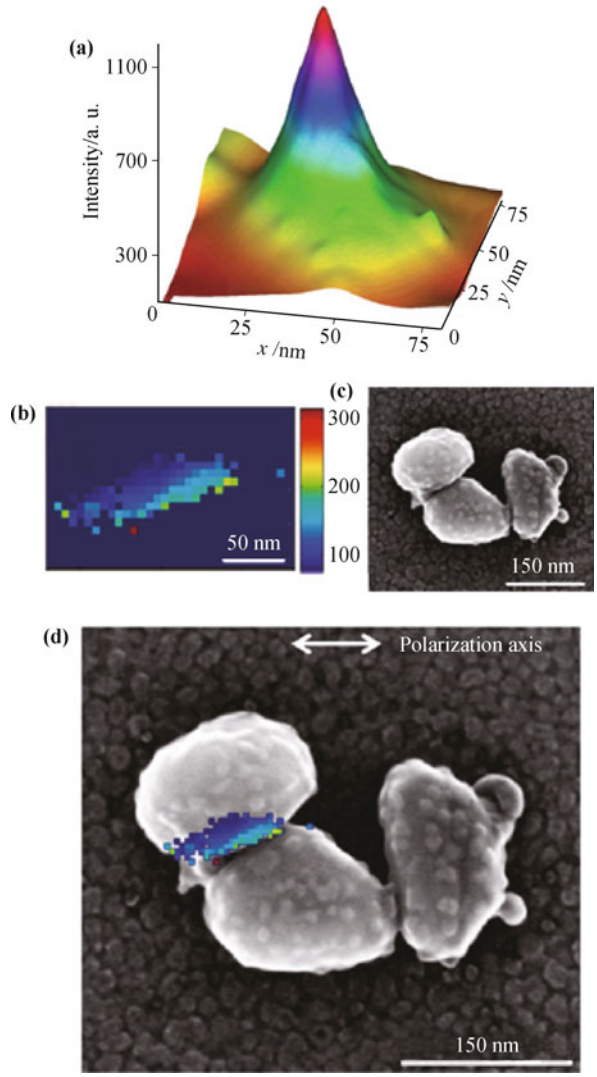

Fig. 3 Measuring hot spots in silver colloidal aggregates by different methods. **(a)** Hot spot map showing fluorescence intensity as a function of spatial origin. Reprinted with permission from Ref. [19], Copyright © 2011 Nature Publishing Group. **(b)** Hot spot map showing SERS intensity as a function spatial origin. **(c)** SEM of the SERS-active nanoparticle aggregate. **(d)** Overlay of hot spot map from (b) on SEM image from (c). Reprinted with permission from Ref. [21], Copyright © 2011 American Chemical Society.

super-resolution images often reproduce structural features of the nanoparticle as determined by electron microscopy, verifying that super-resolution imaging can explore the underlying nanostructures with the relevant nanoscale resolution [20, 21, 29–31, 34]. These results (and others) also suggest that the 2D Gaussian model is sufficiently robust to produce excellent representations of both the shapes of the underlying nanostructures as well as their plasmonic properties, such as electromagnetic hot spots.

3 Alternative PSF models for super-resolution imaging: The dipole PSF

3.1 Problems with the Gaussian model: Lessons from single molecule fluorescence

Although the examples in Section 2.2 serve as convincing evidence that the 2D Gaussian model has value for super-resolution imaging in plasmonics, it is worth considering the applicability of other models. In particular, the single molecule fluorescence community has recognized that using 2D Gaussian fitting can introduce errors in the localization accuracy of an emitter, especially when using high numerical aperture objectives. In the case of a single dipole emitter, the PSF will depend strongly on the orientation of the dipole [43, 44, 53–56]. Figure 4 shows examples of fluorescence emission of single $DiIC_{18}$ molecules immobilized in a polymer film and imaged under total internal reflection illumination using a 1.4 NA objective [53]. In Fig. 4(a), the image is in focus, while in Fig. 4(b), the image is defocused by 300 nm to highlight the asymmetry inherent to emitting dipoles at a dielectric interface. Importantly, the shape of the PSF depends strongly on the orientation of the emitting dipole, with out-of-plane emitters having a characteristic "donut" pattern (as seen as the top emitter in both panels), and in-plane emitters showing wings that reflect their orientation within the sample plane. Even if this pattern is less obvious in the focused images, the PSFs have slight asymmetries in their shapes that are related to the orientation of the dipole emitter.

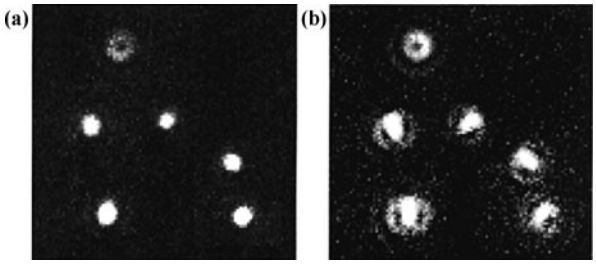

Fig. 4 Fluorescence from single molecules in a polymer film. Image is **(a)** in-focus and **(b)** defocused by 300 nm. Reprinted with permission from Ref. [53], Copyright © 1999 American Chemical Society.

To explore how fitting a dipole PSF with a 2D Gaussian affects localization accuracy, Selvin and coworkers calculated the characteristic dipole emission patterns from a collection of molecules [45]. To do this, they calculate the z-component of the Poynting vector associated with the emitter imaged through the relevant optics and projected onto an imaging CCD with fixed pixel size. The z-component of the Poynting vector (S) is calculated according to Eq. (2) [44–56]:

$$S = \frac{c}{8\pi}\hat{e}_z(\boldsymbol{E} \times \boldsymbol{B}^*) \tag{2}$$

In this expression, c is the speed of light, and $\boldsymbol{E}$ and $\boldsymbol{B}$ are the electric and magnetic fields, respectively, of the emitter. Unlike the 2D Gaussian, the dipole PSF calculation is not a single analytical expression, and must be evaluated for each position on the CCD camera.

For each PSF calculation, the centroid was fixed at some known position (x_{actual} and y_{actual}) and various inputs for the azimuthal (in-plane) and axial (out-of-plane, or inclination) angles were chosen [45]. The resulting PSF was then fit to a 2D Gaussian, and the centroid value of the fit was determined (x_{fit} and y_{fit}). By repeating this process for a population of theoretical molecules with fixed out-of-plane angles and varying in-plane angles, the authors could calculate the average mean-squared-displacement of the centroid position (σ^2) in both x and y, where $\langle\sigma^2\rangle = \langle(x_{\text{fit}} - x_{\text{actual}})^2\rangle = \langle(y_{\text{fit}} - y_{\text{actual}})^2\rangle$ (due to the symmetry of the system, the differences in both x and y should be equivalent, for a large enough population of molecules). Figure 5 shows the results of these calculations as a function of the out-of-plane dipole angles, as well as different experimental parameters such as numerical aperture and detector pixel size [45]. In each plot, the number of emitted photons is also varied from 500 to infinity. These results show that the error in the localization accuracy using a 2D Gaussian fit can exceed 10 nm, especially when relatively few photons are emitted. The localization inaccuracy is further exacerbated when the image is out-of-focus or optical aberrations are present [46, 57]. Thus, a 2D Gaussian model may yield significant errors in the localization accuracy of a single emitting dipole, and the more rigorous dipole PSF should be used for fitting single-molecule super-resolution data with maximum accuracy [45, 46].

Unlike the 2D Gaussian, which has six fitting parameters associated with it (z_0, I_0, x_0, y_0, s_x, s_y as defined in Section 2.1), dipole PSF calculations have (at least) eleven input parameters. Typically, these can be described as static parameters that are dictated by the experiment and fit parameters that are specific to each emitter. The static parameters include numerical aperture, total magnification of the system, the size of each pixel in the imaging CCD, the position of the focus, and the refractive indices of the sample environment, substrate, and imaging medium. The fit parameters include the distance of the emitter from the substrate surface, the wavelength of the emission, the in-plane and out-of-plane dipole angles, the background intensity, and the

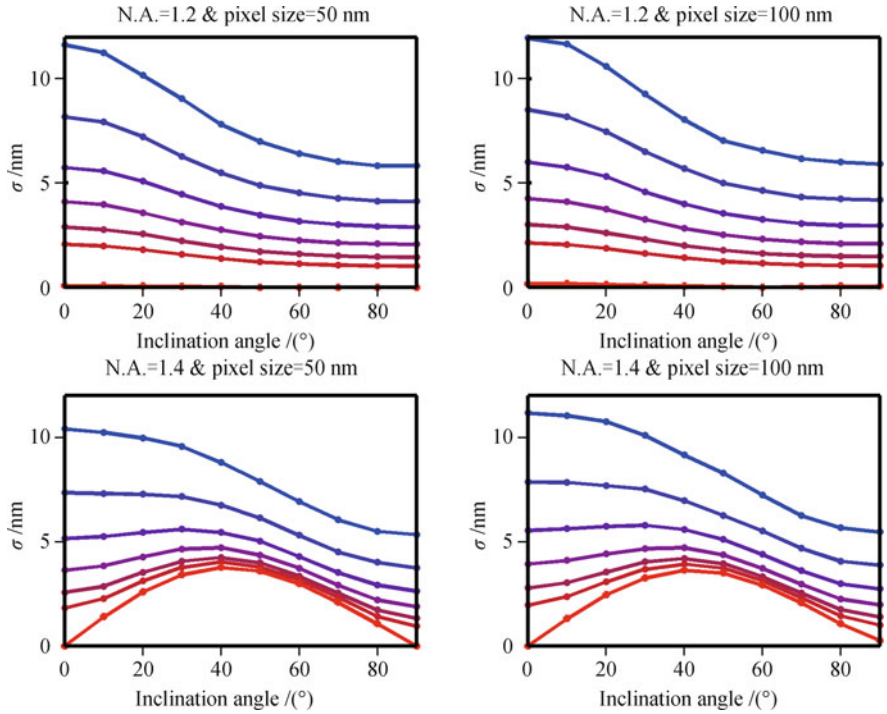

Fig. 5 Calculated error in the centroid using a 2D Gaussian fitting function as a function of out-of-plane dipole angle. Each graph shows calculations for different number of emitted photons. From top to bottom: 500, 1000, 2000, 4000, 8000, 16000, and infinite. Reprinted with permission from Ref. [45], Copyright © 2006 The Optical Society of America.

number of emitted photons. For localizing the position of the emitter, the centroid position must also be included, bringing the number of adjustable parameters to (at least) thirteen. In most cases, assumptions can be made about the system with respect to the fit parameters (for example, emission wavelength), but this still represents a large parameter space for fitting relative to the 2D Gaussian function. Thus, despite the improved localization accuracy of the dipole PSF fit, the 2D Gaussian remains the preferred model because of the reduced computational expense.

In addition to the choice of the fitting model, the algorithm used for evaluating the fit must also be considered. While many researchers use least squares minimization for PSF fitting, others have reported that maximum likelihood estimators yield vastly superior results, with precisions down to the theoretical limit as determined by information theory [58, 59]. Development of new, less computationally expensive fitting algorithms has been the topic of a number of recent publications; however, most of these approaches still use the simpler 2D Gaussian or Airy disk function to model the PSF of the emitter [60–63]. Rather than summarize all of the recent approaches for super-resolution imaging, we will focus here on the potential applicability of dipole PSFs for fitting plasmon-mediated emission events.

3.2 Dipole PSF models in single nanoparticle scattering/luminescence

Having shown that localizing single fluorescent molecules by fitting their PSF to a 2D Gaussian introduces significant error into the fit accuracy, the question now becomes how these results apply to super-resolution imaging in plasmonic systems. Most plasmonic nanoparticles support multiple plasmon modes: dipolar, quadrupolar, etc.; however, in most cases, the dipole mode is the dominant scattering mode regardless of nanoparticle shape (sphere, rod, etc.) [14, 64]. In principle, this dipole mode is analogous to a single radiating dipole, as described in Section 3.1, and should have a dipole PSF. However, how the dipole plasmon scattering is imaged in the far-field will depend very strongly on the shape of the nanostructure and the polarization of the excitation.

We begin by considering scattering from a gold nanorod. Gold nanorods support three dipole modes: two transverse modes associated with the short (width and depth) dimensions and one longitudinal mode associated with the length dimension. Given that the longitudinal dipole mode scatters much more strongly than the transverse modes, we expect a far-field image of a gold nanorod to appear similar to a single dipole [64]. To illustrate this, Fig. 6 shows a dark field image of a gold

nanorod with varying degrees of defocusing [64]. As with the single molecule example shown in Fig. 4, significant asymmetry is observed in the shape of the diffraction-limited image, indicative of the dominance of the longitudinal dipole mode. Similar dipolar behavior from nanorods has been reported by other groups, using both scattering and luminescence from the nanoparticle [33, 65–67]. By fitting the experimental diffraction-limited image to a single dipole PSF model, the 3-dimensional orientation of the nanorod can be determined, although Wu and coworkers have noted that the fits are superior when three orthogonal dipole modes are included in the model [65]. Because of this strong dipolar character in the scattering of a single nanorod, we would expect to introduce localization inaccuracies when using a 2D Gaussian to fit emission from single nanorods. Thus, using a dipole PSF for modeling gold nanorod scattering (or luminescence) should provide superior fit quality in super-resolution imaging. This behavior is expected for any plasmonic nanostructure showing strong anisotropy in its scattering, such that a single dipole plasmon mode dominates all other plasmon modes.

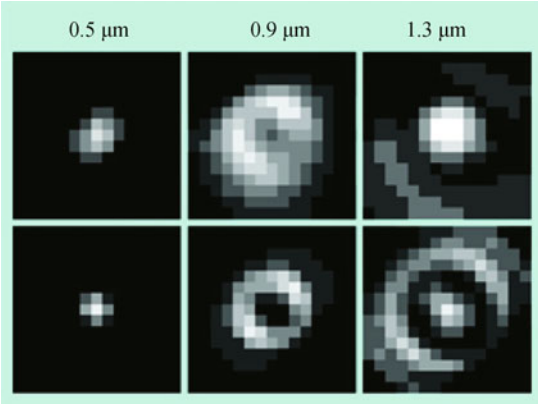

Fig. 6 Measured (*top row*) and calculated (*bottom row*) dark-field scattering from a single gold nanorod under different amounts of defocusing. Reprinted with permission from Ref. [64], Copyright © 2010 American Chemical Society.

If we now consider other shapes, the situation becomes more complicated. For example, a spherical nanoparticle will also support a dipole plasmon mode, but the dipolar plasmon has no preferred orientation due to the infinite rotational symmetry of the sphere. Even when excited by linear polarized light, the resulting scattering from a sphere can be depolarized, such that no single dipole dominates the emission [68]. The situation is similar for other nanoparticle shapes with rotational symmetry that can support multiple dipolar plasmon modes; for example, our group recently showed that a threefold rotationally symmetric silver nanoprism behaves (to a first approximation) like an isotropic scatterer [69, 70]. Mortenson *et al.* have shown that the PSF from a collection of isotropic dipoles (such as a fluorophore-doped nanosphere) is well-modeled by a Gaussian function [58]. Thus, while the dipole PSF model is most appropriate when fitting far-field scattering or luminescence images from anisotropic nanoparticles, such as nanorods, the 2D Gaussian model may provide sufficient localization accuracy for structures with rotational symmetry like nanospheres or even nanoprisms or nanocubes. This conclusion is consistent with the PHOTON results described in Section 2.2, in which the reconstructed distances between spherical nanoparticles attached to streptavidin agreed extremely well with the predicted distances [20].

3.3 Dipole PSF models in SERS

Next, we will consider plasmon-mediated emission processes, in which a molecule is located at or near the nanoparticle surface. We begin with SERS where the emission is strongly coupled into and radiated into the far-field by the plasmon modes of the underlying nanostructure [71]. We will focus here on aggregated nanostructures, which have electromagnetic hot spots within the junctions between adjacent nanoparticles and are frequently used in SERS experiments.

In the case of a nanoparticle dimer, the longitudinal dipole plasmon mode (oriented along the long axis of the dimer) is well-known to dominate the SERS emission, much like the anisotropic nanorods described in the previous section [16, 72] To determine whether this dipole-like emission could be captured by standard wide-field imaging, our group imaged individual SERS-active nanoparticle dimers labeled with ∼1 Rhodamine 6G molecule per aggregate [73]. Figure 7 shows several examples of the resulting diffraction-limited spots, which show remarkable similarity to the single molecule images shown in Fig. 4. However, in this example, we had sufficient signal-to-noise to observe the side lobes without the need for defocusing the images. Next, we used correlated atomic force microscopy (AFM) to measure the structure of the SERS-active nanoparticles. From the AFM images, we determined an in-plane and out-of-plane angle for the nanostructure based on the orientation of the long axis of the dimer and the nanoparticle height asymmetry, respectively. We then calculated the theoretical dipole PSF by modeling the dimer as a single dipole oriented at the in- and out-of-plane angles determined by AFM. The resulting calculated dipole PSFs are shown in Fig. 7 (right column) and show remarkable agreement with the experimentally-measured counterparts (Fig. 7, center), which suggests that a dipole PSF model may be appropriate for SERS-active nanoparticle dimers [73].

We note that the calculations shown in the right column of Fig. 7 are based purely upon the geometric parameters of the nanoparticles, as determined by AFM, and are not fits to the experimental data. Nonetheless, the agreement between the calculated single dipole PSF and the SERS emission is extremely strong, suggesting that the single dipole model may be more accurate for determining the centroid position in super-resolution imaging.

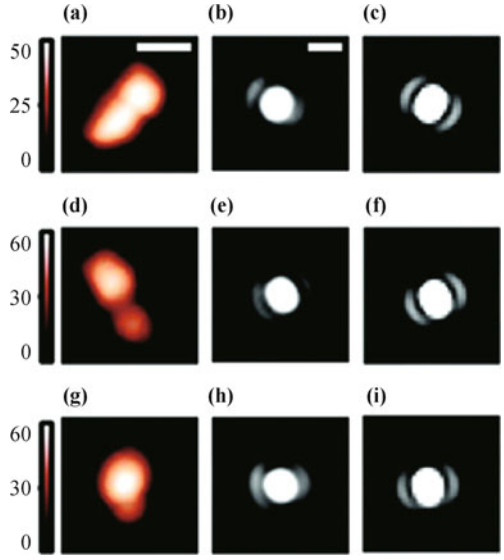

Fig. 7 AFM images (*left column*), measured SERS images (*center column*), and calculated dipole PSF (*right column*) for three different SERS-active nanoparticle dimers. Reprinted with permission from Ref. [73], Copyright © 2011 American Chemical Society.

On the other hand, higher order aggregates present more of a challenge. Figure 8 shows experimental images of several different SERS-active aggregates labeled with multiple Nile Blue molecules [74]. As before, the dimer nanostructure shows a strong dipole-like emission pattern, despite the higher number of SERS reporter molecules adsorbed to the nanoparticle surface. This dipolar emission pattern is preserved whether the SERS is excited with 532 nm or 642 nm light, further supporting the dominance of the longitudinal dipole plasmon mode in determining the SERS emission properties. For comparison, two trimer nanostructures are also included and show markedly different behavior. The bent trimer in Fig. 8(d) also shows dipole-like character when excited at 642 nm [Fig. 8(e)], but the lobes rotate when 532 nm excitation is used [Fig. 8(f)]. The clustered trimer in Fig. 8(g) shows a symmetric emission pattern under 642 nm excitation [Fig. 8(h)], with a low-intensity ring-like pattern surrounding the central high intensity spot. In both of the trimer cases in Fig. 8, multiple plasmon modes are contributing to the emission, which becomes apparent in the non-single dipole properties of the experimental diffraction-limited images.

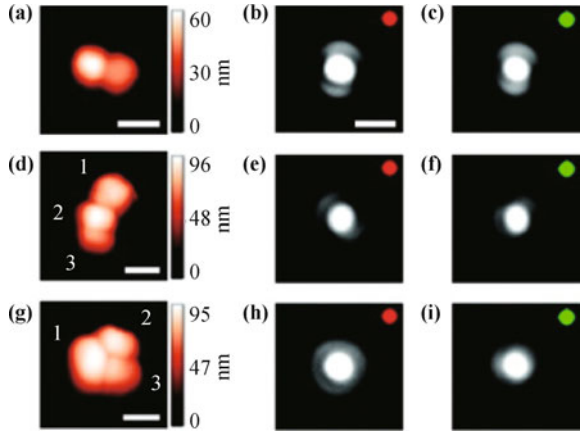

Fig. 8 AFM images (*left column*), measured SERS emission pattern with 642 nm excitation (*center column*), and measured SERS emission pattern with 532 nm excitation (*right column*) for three different SERS-active nanoparticle aggregates. Reprinted with permission from Ref. [74], Copyright © 2012 American Chemical Society.

This phenomenon was also explored by Käll and coworkers, using a slightly modified imaging geometry. Rather than directly imaging the SERS emission on a CCD placed at the imaging plane of the microscope, they imaged the SERS at the Fourier plane of the microscope (Fig. 9) [17]. The Fourier plane allows the angular distribution of radiation to be mapped. The radial coordinate of a Fourier image reflects the angle at which light is emitted by the nanostructure, while the angular coordinate represents the location of the emission in space. Thus, intensity in the center of the image corresponds to light traveling parallel to the optical axis of the microscope, while light on the edges reflects higher angle emission. For the SERS-active dimer shown in Fig. 9(A), high angle emission is observed only at specific angles along the angular coordinate, which are perpendicular to the long-axis of the nanoparticle dimer. This type of Fourier plane image is consistent with dipolar emission [55], and once again confirms that SERS emission from a dimer is dominated by the longitudinal dipolar plasmon. For comparison, the Fourier plane image of SERS from a clustered trimer is shown in Fig. 9(B) [17]. Similar to the SERS image from Fig. 8(h), the high angle emission is symmetric and shows a ring-like pattern, indicating that the emission does not behave like a single dipole, but is coupled to multiple plasmon modes.

Figure 10 shows the calculated Fourier plane images based on the structures of the two nanoparticle aggregates [17]. In these calculations, the dipole PSF is calculated as previously described, but then projected into the Fourier plane, rather than the image plane. For the dimer

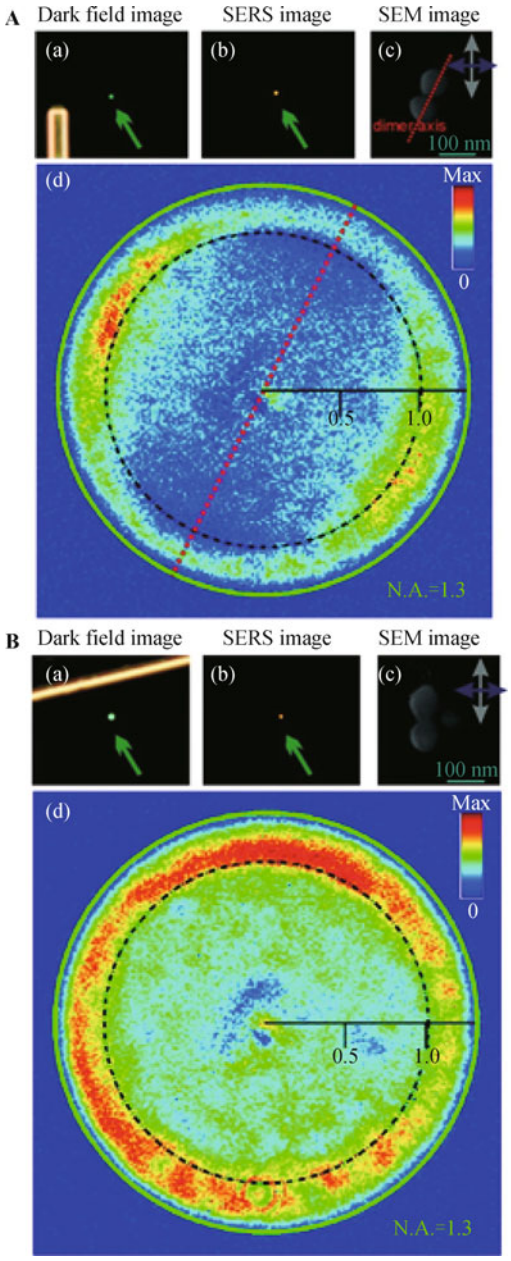

Fig. 9 **(A-a)** Dark field image, **(A-b)** SERS image and **(A-c)** SEM image of a SERS-active nanoparticle dimer. **(A-d)** Fourier plane image of the SERS emission. **(B)** Same as **(A)** but for a nanoparticle trimer. Reprinted with permission from Ref. [17], Copyright © 2011 American Chemical Society.

modeled as a single dipole aligned along the longitudinal axis of the nanostructure [Fig. 10(a)], there is excellent agreement between the calculated [Fig. 10(b)] and experimentally measured [Fig. 9(A)] patterns. For the clustered trimer, the calculation is modeled as the sum of three incoherent dipole modes, each pointing along an individual nanoparticle junction as indicated by the red arrows in Fig. 10(c). As before, the agreement between the calculated [Fig. 10(d)] and measured [Fig. 9(B)] Fourier plane images is clear. These data indicate that it may be possible to model SERS emission as a single (or sum of) dipole PSF(s), and calculate the centroid position following the approach described by the single molecule fluorescence literature [17]. Thus, localization accuracy may be improved in the super-resolution SERS data shown in Section 2.2, simply by using a more sophisticated model.

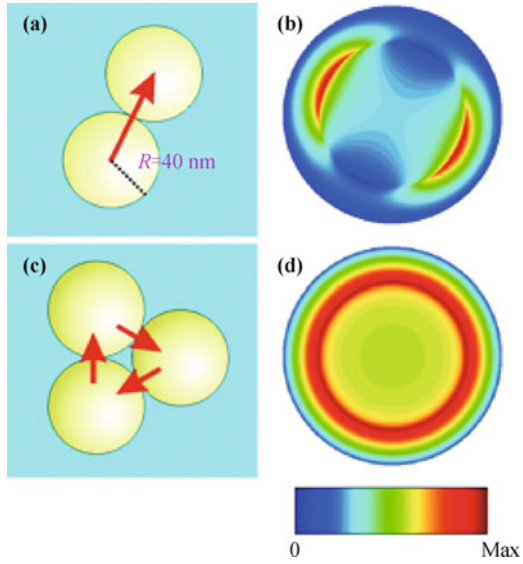

Fig. 10 Calculated Fourier plane images for various nanoparticle clusters based on dipole PSFs. **(a)** Nanoparticle dimer modeled as a single dipole as indicated. **(b)** Calculated Fourier plane image for the dimer from (a). **(c)** Nanoparticle trimer modeled as the sum of three incoherent dipoles as indicated. **(d)** Calculated Fourier plane image for the trimer from (c). Reprinted with permission from Ref. [17], Copyright © 2011 American Chemical Society.

While the dipole PSF model seems like a promising approach for finding the SERS centroid based on the data presented here, there are two major caveats. The first is that we must know the structure of the underlying nanoparticle in order to create the appropriate model. For example, the two trimer nanostructures shown in Fig. 8 have vastly different local structures, with the trimer in Fig. 8(d) having two junctions and the trimer in Fig. 8(g) having three junctions. Thus, we need to know the structure of the nanoparticle in order to build a reasonable dipole PSF model, such as the one shown in Fig. 10(c). The second caveat is that each junction in a higher order aggregate may not be contributing equally, making it important to include the dipole strength in the overall model when multiple modes are contributing [75]. For homogenous nanoparticles, as modeled in Fig. 10, assumptions can be made based upon the alignment of each junction relative to the polarization of the excitation. However, for more realistic samples (such as the clusters shown in Figs. 8 and 9), the size differences among the three nanoparticles will lead to subtle but important

differences in how well the scattered light couples into the various nanoparticle plasmon modes [15, 76]. This is especially problematic in single molecule SERS, where the junction occupied by the single molecule is expected to dominate the emission, with all other junctions contributing weakly [16, 29, 76]. Thus, we have to consider a weighted sum of different dipole modes when dealing with more realistic nanostructures in order to accurately model the PSF of the plasmon-mediated emission. As a result, the dipole PSF may be appropriate for centroid localization with SERS-active dimers, but may introduce too much additional uncertainty into the calculation for higher order aggregates, offsetting the potential improvement in accuracy over a 2D Gaussian.

3.4 Dipole PSF models in surface-enhanced fluorescence

In surface-enhanced fluorescence, emitters are spaced from the nanoparticle surface by 5–15 nm; thus the fluorescence may not couple efficiently into plasmon modes and may be a convolution of direct far-field emission and plasmon-coupled emission [77]. On first glance, it appears that the lessons from the single molecule fluorescence community (Section 3.1) may directly apply to measuring surface-enhanced fluorescence from single molecules. However, even in the case of direct molecular emission into the far-field, the PSF can be significantly distorted by the presence of the metallic nanostructure [26, 78]. Figure 11 shows calculations of how the angular PSF of a single dipole is perturbed by the presence of a metallic nanowire [26]. In this case, the collection angle of the microscope is highlighted in gray in each polar plot. The resulting distorted dipole PSF depends not only on the position of the molecule on the nanoparticle surface, but also the orientation of the transition dipole of the molecule relative to the nanowire. For example, the PSF of a dipole positioned on the side of the nanowire facing the collection optic will be dominated by low angle emission if the dipole is oriented perpendicular to the optical axis [Fig. 11(B), vii)]; this PSF will most likely be well-described by a 2D Gaussian. On the other hand, if the dipole is oriented parallel to the optical axis [Fig. 11(B), viii)], the PSF will be dominated by high angle emission and will have a pattern similar to the donut shaped emission from Fig. 4. For a dipole located on the opposite side of the nanowire, the situation changes dramatically: minimal emission will be observed if the dipole is oriented perpendicular to the optical axis [Fig. 11(B), i)], but will have sizable emission collected by the objective when oriented parallel to the optical axis [Fig. 11(B), ii)]. The differences in the angular distribution of radiation from each of the fluorophores in these different examples will result in vastly different PSFs in the accompanying fluorescence images.

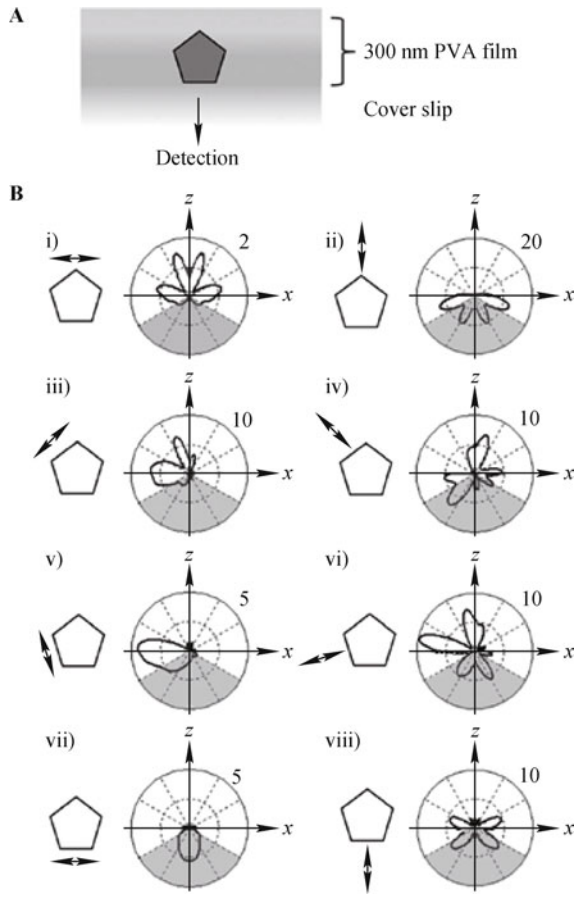

Fig. 11 **(A)** Schematic of a gold nanowire, viewed from the end, immobilized in a PVA film. Fluorescence is detected from the bottom edge as indicated. **(B)** Angular distribution of fluorescence from a radiating dipole positioned near the nanowire surface as indicated. The gray shaded region represents the collection angle of the objective. Reprinted with permission from Ref. [26], Copyright © 2011 John Wiley and Sons.

As with the case of SERS, the question becomes: how much do you need to know about the system in order to accurately model the PSF? From the calculations, it appears that we need to know both the location of the emitter as well as its orientation relative to the nanoparticle surface in order to properly model the PSF. Returning to the previous example of super-resolution imaging of fluorescently-labeled surface-bound ligands on nanoparticle surfaces from Fig. 2, we note that this image was constructed by measuring emission from >100 individual molecules [34]. Thus, knowing the precise orientation and position of each fluorophore represents a distinct experimental challenge. By using floppy linkers, we can negate some of the orientation effects by averaging over all possible molecular orientations. However, we have no straight-

forward way to discriminate the position of the emitter on the nanowire surface, requiring us to introduce additional fitting parameters into the PSF calculation and add to the computational expense. Moreover, the excellent agreement between the reconstructed image and the SEM of the nanowire structure in Fig. 2 suggests that a 2D Gaussian may be sufficiently accurate for modeling single molecule fluorescence data in this system [34].

A conflicting view, however, was reported by Uji-i and coworkers, who also used super-resolution imaging of fluorescently-labeled surface-bound ligands to reconstruct the shape of nanowires [26]. In their data, the width of the reconstructed nanowire image was much larger than the actual geometry of the nanostructure, and they hypothesized that this discrepancy was due to the distortion of the fluorescent PSFs close to the nanowire surface. This difference between the two data sets may be due to the fluorophore spacing (we used DNA to space the fluorophores from the surface, while they used a biotin-streptavidin linkage), choice of fluorophore (the small organic fluorophore TAMRA versus a large photoactivated protein), rotational mobility of the fluorophore (ours was tethered by a floppy 6-carbon chain, while the protein is much more rigid), differences in nanowire material (gold versus silver), or even choice of fluorophore signal modulation strategy (triplet state shelving versus light-activated photoswitch) [26, 34]. While more work is needed to distinguish why the 2D Gaussian model was more successful in one experiment over another, it is clear that distortion of the fluorescence by the nearby metal nanostructure must be considered before choosing a fitting approach for super-resolution imaging.

4 Outlook and conclusion

In this Perspective, we considered the applicability of a dipole PSF to improve localization accuracy in fitting plasmon-mediated emission events for super-resolution imaging. Based on results from the single-molecule fluorescence community, we expect that the conventional 2D Gaussian may introduce error into the centroid position, which may be mitigated by a more mathematically rigorous choice of model. Given the dominance of the dipole plasmon mode in many different plasmonic systems, using a dipole PSF-based fitting model seemed a logical first step. We reviewed several different systems in this manuscript and found that there were indicators that a dipole-based model might, indeed, serve to improve localization accuracy in centroid determination for plasmonic systems.

However, before we suggest moving exclusively towards dipole PSF models for plasmonic super-resolution imaging, we must consider several important factors. First, the PSF-based model represents considerable computational expense for fitting super-resolution data. In our hands, fitting a single frame of data to a Gaussian versus a dipole PSF takes 1 second versus 15 minutes (we note that this is not a computationally optimized value, although it gives the reader a sense of the difference in time scale). This is because the E and B-fields must be recalculated and propagated through the various optics for each iteration of the PSF calculation in order to converge to an optimized fit.

Second, we have found that for most cases, knowledge of the plasmonic nanoparticle structure is necessary to define the correct PSF model. For example, in the case of the SERS data, the PSF is extremely sensitive to the number and organization of the various nanoparticles in the aggregate, and depends also on the number, position and orientation of the SERS probes on the surface. A similar probe dependence was noted in the surface-enhanced fluorescence data, where the location and orientation of the fluorescent molecule could dramatically influence the PSF. In fact, the most straightforward application of the dipole PSF was in the case of direct scattering or luminescence of metallic nanorods, and even these structures are not perfectly modeled by a single dipole PSF. Without knowing something about the structure under study, the use of a dipole PSF is nearly impossible to implement, simply due to the numerous degrees of freedom associated with both the fit and the number of potential plasmon modes associated with many nanostructures.

At present, how best to model the PSFs from plasmonic nanostructures remains an open (and exciting) question. For now, theory may be the best way to approach this problem, using techniques like the finite difference time domain (FDTD) calculations shown in Fig. 11 [26]. By calculating the PSF of a model nanoparticle (or coupled nanoparticle-molecule emitter) and propagating the contributions of various plasmon modes from the near-field to a final far-field image, we can fit that image to a 2D Gaussian to determine the localization accuracy in the centroid fit (as in the work from Selvin and coworkers, shown in Fig. 5) [45]. These types of calculations may allow us to determine situations where the 2D Gaussian is simply inappropriate and another model must be used. Moreover, by bringing new theoretical perspective to this problem, we may be able to move beyond the somewhat over-simplified picture of an emitting dipole when considering plasmonic PSFs.

In the meantime, the good news is that the 2D Gaus-

sian has performed at a sufficiently high level to yield excellent agreement between the structure of the nanoparticle and the location of the subsequent emission in multiple systems. As such, experimentalists can continue to use the 2D Gaussian as a starting point for their super-resolution imaging studies, as long as they exercise caution when assigning meaning to their data. For this reason, correlated optical and structural studies will remain of critical importance when analyzing super-resolution imaging data.

Acknowledgements I gratefully acknowledge Eric Titus for critical reading of this manuscript, and Karole Blythe and Maggie Weber for the data in Fig. 1. This material is based on work supported by the Welch Foundation under Award No. F-1699 and the Air Force Office of Scientific Research under AFOSR Award No. FA9550-09-0112.

References and notes

1. K. A. Willets and R. P. Van Duyne, Localized surface plasmon resonance spectroscopy and sensing, *Annu. Rev. Phys. Chem.*, 2007, 58(1): 267
2. N. J. Halas, S. Lal, W. S. Chang, S. Link, and P. Nordlander, Plasmons in strongly coupled metallic nanostructures, *Chem. Rev.*, 2011, 111(6): 3913
3. J. A. Dionne and H. A. Atwater, Plasmonics: Metal-worthy methods and materials in nanophotonics, *MRS Bull.*, 2012, 37(8): 717
4. S. Lal, J. H. Hafner, N. J. Halas, S. Link, and P. Nordlander, Noble metal nanowires: From plasmon waveguides to passive and active devices, *Acc. Chem. Res.*, 2012, 45(11): 1887
5. S. A. Maier, Plasmonics: Metal nanostructures for subwavelength photonic devices, *IEEE J. Sel. Top. Quantum Electron.*, 2006, 12(6): 1214
6. M. Righini, P. Ghenuche, S. Cherukulappurath, V. Myroshnychenko, F. J. García de Abajo, and R. Quidant, Nano-optical trapping of Rayleigh particles and Escherichia coli bacteria with resonant optical antennas, *Nano Lett.*, 2009, 9(10): 3387
7. K. C. Toussaint, M. Liu, M. Pelton, J. Pesic, M. J. Guffey, P. Guyot-Sionnest, and N. F. Scherer, Plasmon resonance-based optical trapping of single and multiple Au nanoparticles, *Opt. Express*, 2007, 15(19): 12017
8. A. J. Haes, C. L. Haynes, A. D. McFarland, G. C. Schatz, R. P. van Duyne, and S. Zou, Plasmonic materials for surface-enhanced sensing and spectroscopy, *MRS Bull.*, 2005, 30(5): 368
9. R. S. Golightly, W. E. Doering, and M. J. Natan, Surface-enhanced Raman spectroscopy and homeland security: A perfect match? *ACS Nano*, 2009, 3(10): 2859
10. P. L. Stiles, J. A. Dieringer, N. C. Shah, and R. P. Van Duyne, Surface-enhanced Raman spectroscopy, *Annu. Rev. Anal. Chem.*, 2008, 1(1): 601
11. M. Moskovits, Surface-enhanced Raman scattering, *Topics in Applied Physics*, 2006, 103: 1
12. E. Fort and S. Gresillon, Surface enhanced fluorescence, *J. Phys. D*, 2008, 41(1): 013001/1
13. C. D. Geddes, K. Aslan, I. Gryczynski, J. Malicka, and J. R. Lakowicz, Noble metal nanostructure for metal-enhanced fluorescence, *Annual Reviews in Fluorescence*, 2004, 1: 365
14. K. L. Kelly, E. Coronado, L. L. Zhao, and G. C. Schatz, The optical properties of metal nanoparticles: The influence of size, shape, and dielectric environment, *J. Phys. Chem. B*, 2003, 107(3): 668
15. K. L. Wustholz, A. I. Henry, J. M. McMahon, R. G. Freeman, N. Valley, M. E. Piotti, M. J. Natan, G. C. Schatz, and R. P. Van Duyne, Structure-activity relationships in gold nanoparticle dimers and trimers for surface-enhanced Raman spectroscopy, *J. Am. Chem. Soc.*, 2010, 132(31): 10903
16. T. Shegai, Z. Li, T. Dadosh, Z. Zhang, H. Xu, and G. Haran, Managing light polarization via plasmon-molecule interactions within an asymmetric metal nanoparticle trimer, *Proc. Natl. Acad. Sci. USA*, 2008, 105(43): 16448
17. T. Shegai, B. Brian, V. D. Miljković, and M. Käll, Angular distribution of surface-enhanced Raman scattering from individual Au nanoparticle aggregates, *ACS Nano*, 2011, 5(3): 2036
18. S. M. Stranahan and K. A. Willets, Super-resolution optical imaging of single-molecule SERS hot spots, *Nano Lett.*, 2010, 10(9): 3777
19. H. Cang, A. Labno, C. Lu, X. Yin, M. Liu, C. Gladden, Y. Liu, and X. Zhang, Probing the electromagnetic field of a 15-nanometre hotspot by single molecule imaging, *Nature*, 2011, 469(7330): 385
20. T. Huang and X. H. Nancy Xu, Multicolored nanometre-resolution mapping of single protein-ligand binding complexes using far-field photostable optical nanoscopy (PHOTON), *Nanoscale*, 2011, 3(9): 3567
21. M. L. Weber and K. A. Willets, Correlated super-resolution optical and structural studies of surface-enhanced Raman scattering hot spots in silver colloid aggregates, *J. Phys. Chem. Lett.*, 2011, 2(14): 1766
22. F. Balzarotti and F. D. Stefani, Plasmonics meets far-field optical nanoscopy, *ACS Nano*, 2012, 6(6): 4580
23. M. Davies, A. Wochnik, F. Feil, C. Jung, C. Bräuchle, C. Scheu, and J. Michaelis, Synchronous emission from nanometric silver particles through plasmonic coupling on silver nanowires, *ACS Nano*, 2012, 6(7): 6049
24. J. W. Ha, K. Marchuk, and N. Fang, Focused orientation and position imaging (FOPI) of single anisotropic plasmonic nanoparticles by total internal reflection scattering microscopy, *Nano Lett.*, 2012, 12(8): 4282
25. T. Huang, L. M. Browning, and X. H. N. Xu, Far-field photostable optical nanoscopy (PHOTON) for real-time super-resolution single-molecular imaging of signaling pathways of single live cells, *Nanoscale*, 2012, 4(9): 2797

26. H. Lin, S. P. Centeno, L. Su, B. Kenens, S. Rocha, M. Sliwa, J. Hofkens, and H. Uji-i, Mapping of surface-enhanced fluorescence on metal nanoparticles using super-resolution photoactivation localization microscopy, *ChemPhysChem*, 2012, 13(4): 973
27. L. B. Sagle, L. K. Ruvuna, J. M. Bingham, C. Liu, P. S. Cremer, and R. P. Van Duyne, Single plasmonic nanoparticle tracking studies of solid supported bilayers with ganglioside lipids, *J. Am. Chem. Soc.*, 2012, 134(38): 15832
28. E. J. Titus, M. L. Weber, S. M. Stranahan, and K. A. Willets, Super-resolution SERS imaging beyond the single-molecule limit: An isotope-edited approach, *Nano Lett.*, 2012, 12(10): 5103
29. M. L. Weber, J. P. Litz, D. J. Masiello, and K. A. Willets, Super-resolution imaging reveals a difference between SERS and luminescence centroids, *ACS Nano*, 2012, 6(2): 1839
30. X. Zhou, N. M. Andoy, G. Liu, E. Choudhary, K. S. Han, H. Shen, and P. Chen, Quantitative super-resolution imaging uncovers reactivity patterns on single nanocatalysts, *Nat. Nanotechnol.*, 2012, 7(4): 237
31. N. M. Andoy, X. Zhou, E. Choudhary, H. Shen, G. Liu, and P. Chen, Single-molecule catalysis mapping quantifies site-specific activity and uncovers radial activity gradient on single 2D nanocrystals, *J. Am. Chem. Soc.*, 2013, 135(5): 1845
32. L. Wei, C. Liu, B. Chen, P. Zhou, H. Li, L. Xiao, and E. S. Yeung, *Analytical Chemistry*, 2013, Ahead of Print
33. K. Marchuk, J. W. Ha, and N. Fang, Three-dimensional high-resolution rotational tracking with superlocalization reveals conformations of surface-bound anisotropic nanoparticles, *Nano Lett.*, 2013, 13(3): 1245
34. K. L. Blythe, K. M. Mayer, M. L. Weber, and K. A. Willets, Ground state depletion microscopy for imaging interactions between gold nanowires and fluorophore-labeled ligands, *Phys. Chem. Chem. Phys.*, 2013, 15(12): 4136
35. W. E. Moerner, Microscopy beyond the diffraction limit using actively controlled single molecules, *J. Microsc.*, 2012, 246(3): 213
36. K. A. Willets, S. M. Stranahan, and M. L. Weber, Shedding light on surface-enhanced Raman scattering hot spots through single-molecule super-resolution imaging, *J. Phys. Chem. Lett.*, 2012, 3(10): 1286
37. A. Yildiz, J. N. Forkey, S. A. McKinney, T. Ha, Y. E. Goldman, and P. R. Selvin, Myosin V walks hand-over-hand: Single fluorophore imaging with 1.5-nm localization, *Science*, 2003, 300(5628): 2061
38. G. P. Wiederrecht, Near-field optical imaging of noble metal nanoparticles, *Eur. Phys. J.: Appl. Phys.*, 2004, 28(1): 3
39. K. I. Willig, B. Harke, R. Medda, and S. W. Hell, STED microscopy with continuous wave beams, *Nat. Methods*, 2007, 4(11): 915
40. Y. Sivan, Y. Sonnefraud, S. Kena-Cohen, J. B. Pendry, and S. A. Maier, *ACS Nano*, 2012, Ahead of Print
41. F. Wei and Z. Liu, Plasmonic structured illumination microscopy, *Nano Lett.*, 2010, 10(7): 2531
42. E. H. Hellen and D. Axelrod, Fluorescence emission at dielectric and metal-film interfaces, *J. Opt. Soc. Am. B*, 1987, 4(3): 337
43. R. M. Dickson, D. J. Norris, and W. E. Moerner, Simultaneous imaging of individual molecules aligned both parallel and perpendicular to the optic axis, *Phys. Rev. Lett.*, 1998, 81(24): 5322
44. M. Bohmer and J. Enderlein, Orientation imaging of single molecules by wide-field epifluorescence microscopy, *J. Opt. Soc. Am. B*, 2003, 20(3): 554
45. J. Enderlein, E. Toprak, and P. R. Selvin, Polarization effect on position accuracy of fluorophore localization, *Opt. Express*, 2006, 14(18): 8111
46. S. Stallinga and B. Rieger, Accuracy of the gaussian point spread function model in 2D localization microscopy, *Opt. Express*, 2010, 18(24): 24461
47. E. Betzig, G. H. Patterson, R. Sougrat, O. W. Lindwasser, S. Olenych, J. S. Bonifacino, M. W. Davidson, J. Lippincott-Schwartz, and H. F. Hess, Imaging intracellular fluorescent proteins at nanometer resolution, *Science*, 2006, 313(5793): 1642
48. M. J. Rust, M. Bates, and X. Zhuang, Sub-diffraction-limit imaging by stochastic optical reconstruction microscopy (STORM), *Nat. Methods*, 2006, 3(10): 793
49. K. Lidke, B. Rieger, T. Jovin, and R. Heintzmann, Superresolution by localization of quantum dots using blinking statistics, *Opt. Express*, 2005, 13(18): 7052
50. J. Fölling, M. Bossi, H. Bock, R. Medda, C. A. Wurm, B. Hein, S. Jakobs, C. Eggeling, and S. W. Hell, Fluorescence nanoscopy by ground-state depletion and single-molecule return, *Nat. Methods*, 2008, 5(11): 943
51. C. Steinhauer, C. Forthmann, J. Vogelsang, and P. Tinnefeld, Superresolution microscopy on the basis of engineered dark states, *J. Am. Chem. Soc.*, 2008, 130(50): 16840
52. K. A. Willets and S. M. Stranahan, Single molecule spectroscopy and superresolution imaging V, in: *Proceedings of SPIE* 2012, 8228: 82280P-82280P-8
53. A. P. Bartko and R. M. Dickson, Imaging three-dimensional single molecule orientations, *J. Phys. Chem. B*, 1999, 103(51): 11237
54. B. Sick, B. Hecht, and L. Novotny, Orientational imaging of single molecules by annular illumination, *Phys. Rev. Lett.*, 2000, 85(21): 4482
55. M. A. Lieb, J. M. Zavislan, and L. Novotny, Single-molecule orientations determined by direct emission pattern imaging, *J. Opt. Soc. Am. B*, 2004, 21(6): 1210
56. D. Patra, I. Gregor, and J. Enderlein, Image analysis of defocused single-molecule images for three-dimensional molecule orientation studies, *J. Phys. Chem. A*, 2004, 108(33): 6836
57. J. Engelhardt, J. Keller, P. Hoyer, M. Reuss, T. Staudt, and S. W. Hell, Molecular orientation affects localization ac-

curacy in superresolution far-field fluorescence microscopy, *Nano Lett.*, 2011, 11(1): 209

58. K. I. Mortensen, L. S. Churchman, J. A. Spudich, and H. Flyvbjerg, Optimized localization analysis for single-molecule tracking and super-resolution microscopy, *Nat. Methods*, 2010, 7(5): 377
59. A. V. Abraham, S. Ram, J. Chao, E. S. Ward, and R. J. Ober, Quantitative study of single molecule location estimation techniques, *Opt. Express*, 2009, 17(26): 23352
60. R. Parthasarathy, Rapid, accurate particle tracking by calculation of radial symmetry centers, *Nat. Methods*, 2012, 9(7): 724
61. S. Wolter, A. Löschberger, T. Holm, S. Aufmkolk, M. C. Dabauvalle, S. van de Linde, and M. Sauer, rapidSTORM: Accurate, fast open-source software for localization microscopy, *Nat. Methods*, 2012, 9(11): 1040
62. L. Zhu, W. Zhang, D. Elnatan, and B. Huang, Faster STORM using compressed sensing, *Nat. Methods*, 2012, 9(7): 721
63. J. Chao, S. Ram, E. S. Ward, and R. J. Ober, Ultrahigh accuracy imaging modality for super-localization microscopy, *Nat. Methods*, 2013, 10(4): 335
64. L. Xiao, Y. X. Qiao, Y. He, and E. S. Yeung, Three dimensional orientational imaging of nanoparticles with darkfield microscopy, *Anal. Chem.*, 2010, 82(12): 5268
65. T. Li, Q. Li, Y. Xu, X. J. Chen, Q. F. Dai, H. Liu, S. Lan, S. Tie, and L. J. Wu, Three-dimensional orientation sensors by defocused imaging of gold nanorods through an ordinary wide-field microscope, *ACS Nano*, 2012, 6(2): 1268
66. F. Wackenhut, A. Virgilio Failla, T. Zuechner, M. Steiner, and A. J. Meixner, Three-dimensional photoluminescence mapping and emission anisotropy of single gold nanorods, *Appl. Phys. Lett.*, 2012, 100(26): 263102/1
67. T. Motegi, H. Nabika, Y. Niidome, and K. Murakoshi, Observation of defocus images of a single metal nanorod, *J. Phys. Chem. C*, 2013, 117(6): 2535
68. N. G. Khlebtsov, A. G. Mel'nikov, V. A. Bogatyrev, A. V. Alekseeva, and B. N. Khlebtsov, Depolarization of light scattered by gold nanospheres and nanorods, *Opt. Spectrosc.*, 2006, 100(3): 448
69. K. A. Koen, M. L. Weber, K. M. Mayer, E. Fernandez, and K. A. Willets, Spectrally-resolved polarization anisotropy of single plasmonic nanoparticles excited by total internal reflection, *J. Phys. Chem. C*, 2012, 116(30): 16198
70. O. Schubert, J. Becker, L. Carbone, Y. Khalavka, T. Provalska, I. Zins, and C. Sönnichsen, Mapping the polarization pattern of plasmon modes reveals nanoparticle symmetry, *Nano Lett.*, 2008, 8(8): 2345
71. L. K. Ausman and G. C. Schatz, On the importance of incorporating dipole reradiation in the modeling of surface enhanced Raman scattering from spheres, *J. Chem. Phys.*, 2009, 131(8): 084708/1
72. H. Xu and M. Käll, Polarization-dependent surface-enhanced Raman spectroscopy of isolated silver nanoaggregates, *ChemPhysChem*, 2003, 4(9): 1001
73. S. M. Stranahan, E. J. Titus, and K. A. Willets, SERS orientational imaging of silver nanoparticle dimers, *J. Phys. Chem. Lett.*, 2011, 2(21): 2711
74. S. M. Stranahan, E. J. Titus, and K. A. Willets, Discriminating nanoparticle dimers from higher order aggregates through wavelength-dependent SERS orientational imaging, *ACS Nano*, 2012, 6(2): 1806
75. D. W. Brandl, N. A. Mirin, and P. Nordlander, Plasmon modes of nanosphere trimers and quadrumers, *J. Phys. Chem. B*, 2006, 110(25): 12302
76. Z. Li, T. Shegai, G. Haran, and H. Xu, Multiple-particle nanoantennas for enormous enhancement and polarization control of light emission, *ACS Nano*, 2009, 3(3): 637
77. T. Ming, H. Chen, R. Jiang, Q. Li, and J. Wang, Plasmon-controlled fluorescence: Beyond the intensity enhancement, *J. Phys. Chem. Lett.*, 2012, 3(2): 191
78. S. Kuhn, U. Hakanson, L. Rogobete, and V. Sandoghdar, Enhancement of single-molecule fluorescence using a gold nanoparticle as an optical nanoantenna, *Phys. Rev. Lett.*, 2006, 97(1): 017402/1